AEROCOM Workshop (10-12 March 2004; Ispra, Italy)

Climate response to aerosol direct and indirect effects with global aerosol radiation-transport model

Toshihiko Takemura[1]
Toru Nozawa[2], Seita Emori[3], Teruyuki Nakajima[4]

1: Research Institute for Applied Mechanics (RIAM), Kyushu University
2: National Institute for Environmental Studies (NIES)
3: Frontier Research System for Global Change (FRSGC)
4: Center for Climate System Research (CCSR), University of Tokyo

Objective

Simulation of climate change by the aerosol direct and indirect effects using the global aerosol model coupled with a mixed-layer ocean GCM.

Model description

SPRINTARS
(Spectral Radiation-Transport Model for Aerosol Species)

Takemura et al. (*JGR, 105, 17853-17873, 2000*)
Takemura et al. (*J. Clim., 15, 333-352, 2002*)

Coupled with CCSR/NIES/FRSGC AGCM

Tracers: black carbon (BC), organic carbon (OC), sulfate, soil dust, sea salt, SO_2, DMS

Emission

- BC, OC: biomass burning, fossil fuel, biofuel, agricultural activity, terpene
- SO_2: fossil fuel, biomass burning, volcano
- DMS: oceanic phytoplankton, land vegetation
- Soil dust: dependence on 10-m height wind, vegetation, soil moisture, snow amount
- Sea salt: dependence on 10-m height wind

Advection

Flux-Form Semi-Lagrangian (FFSL) method
Arakawa-Schubert cumulus convection

Diffusion

Chemical reaction (sulfur)

Gas phase: $DMS+OH \rightarrow SO_2$, $SO_2+OH \rightarrow SO_4^{2-}$
Liquid phase: $S(IV)+O_3 \rightarrow SO_4^{2-}$, $S(IV)+H_2O_2 \rightarrow SO_4^{2-}$
»OH, O_3, H_2O_2: CHASER (*Sudo et al. 2002*)

Deposition

Wet deposition (wash out, rain out)
Re-emission by evaporation of rain
Dry deposition
Gravitational settling

Aerosol direct effect

Distinction of refractive indices, size distributions, and hygroscopic growth among aerosol species.

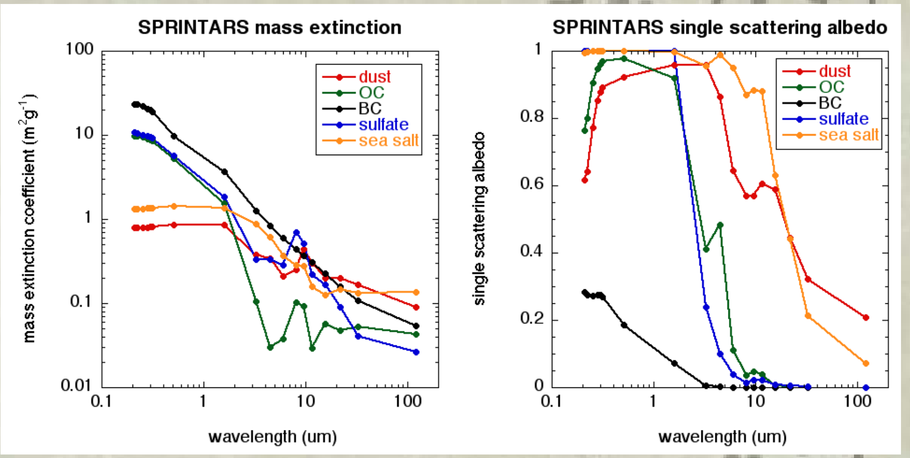

Wavelength dependences of mass extinction efficiency (left) and single scattering albedo (right) for dry particles of each aerosol species.

Aerosol indirect effect

Cloud droplet number concentration N_c

$$N_c = N_a \left[1 + \left\{ f_1(\sigma_a) \left(\frac{A N_a \beta}{3\alpha\omega} \right)^2 + f_2(\sigma_a) \frac{2A^3 N_a \beta \sqrt{G}}{27 B r_m{}^3 (\alpha\omega)^{3/2}} \right\}^{b(\sigma_a)} \right]^{-1}$$

Abdul-Razzak et al. (1998), Ghan et al. (1997)

N_a: aerosol particle number concentration
ω: updraft velocity ($=\overline{\omega} + c\sqrt{TKE}$)
r_m: mode radius of size distribution of aerosol particles
σ_a: standard deviation of size distribution of aerosol particles
A: curvature effect
B: solute effect

Cloud droplet effective radius r_{eff}

→ first indirect effect

$$r_{eff} = k \left(\frac{3}{4\pi\rho_w} \frac{\rho l}{N_c} \right)^{\frac{1}{3}}$$

ρl: cloud water content
ρ_w: water density

Precipitation ratio P

→ second indirect effect

$$P = -\frac{dl}{dt} = \frac{\alpha \rho l^2}{\beta + \gamma \frac{N_c}{\rho l}}$$

α, β, γ: constants

Experimental setting

- Coupled with a mixed-layer ocean model.
- 30-year integration → last 10-year analysis (equilibrium run).
- Resolution: T42 (approx. 2.8 x 2.8 in longitude and latitude), L20.
- Present-day (2000) and pre-industrial (1850) aerosol emission runs.
  Anthropogenic emission data from 1850 to 2000 re-edited by our GCM group (*Nozawa et al.*).
- Constant greenhouse gas concentrations in 2000 level.

Emission data

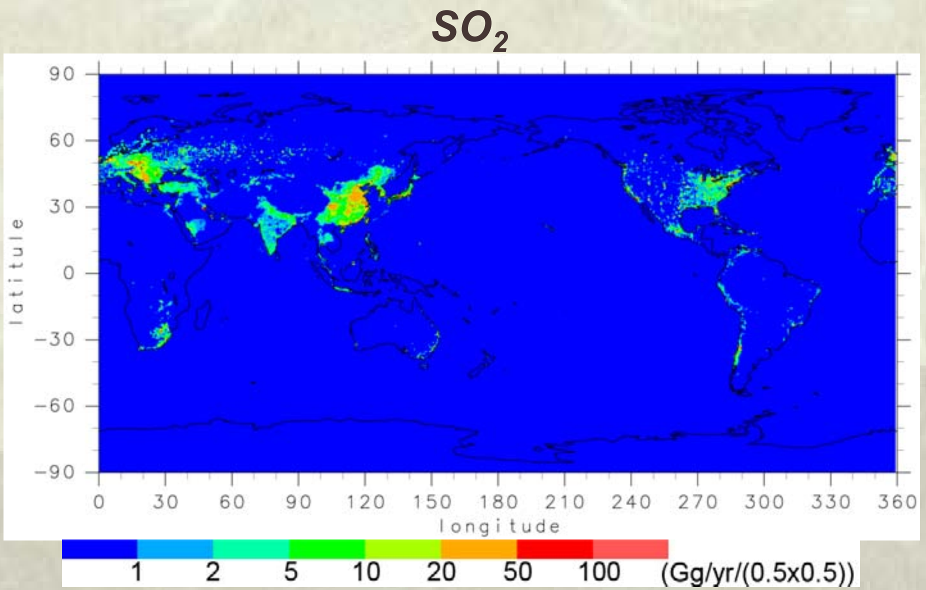

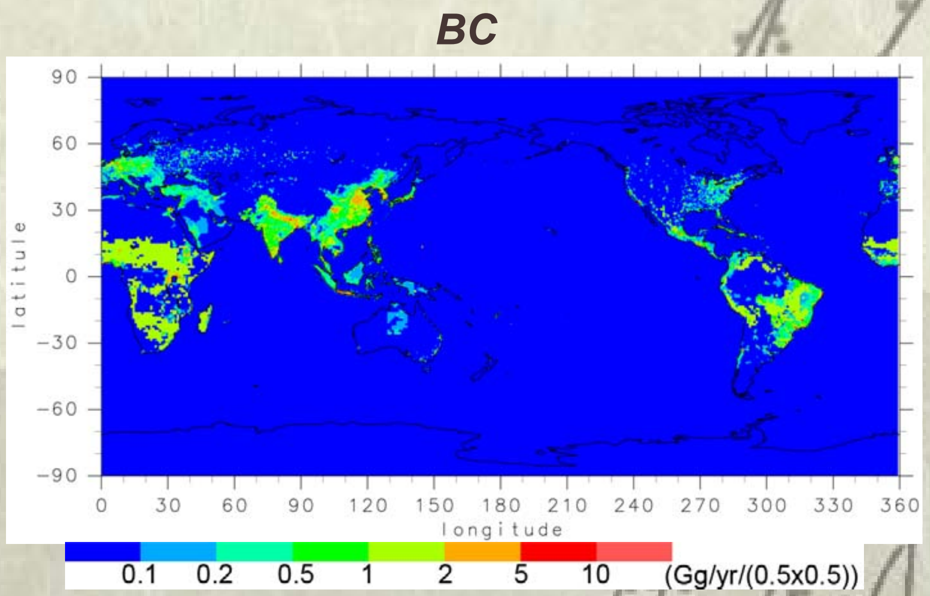

Anthropogenic emission data in 2000 for SO_2 (left) and BC (right) (*NIES*).

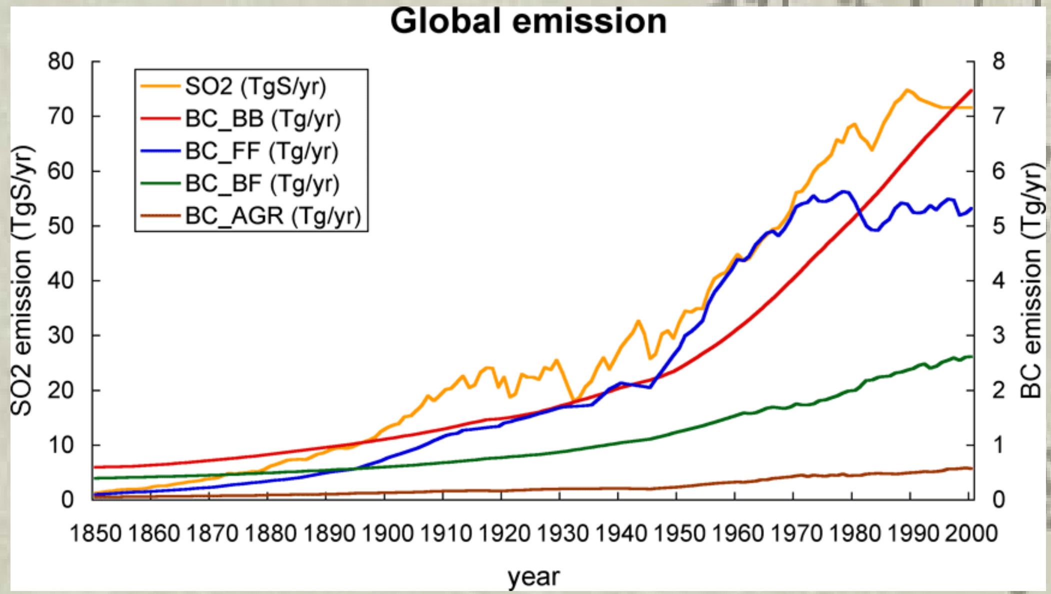

Emission of anthropogenic SO_2 and BC from biomass burning, fossil fuel, biofuel, and agricultural activity from 1850 to 2000 (*NIES*).

Emission data

Historical Emission of Anthropogenic SO_2

- Country-base historical inventory (*Lefohn et al., 1999*)
- Gridded into 0.5º x 0.5º resolution with population distribution data obtained from CIESIN and HYDE

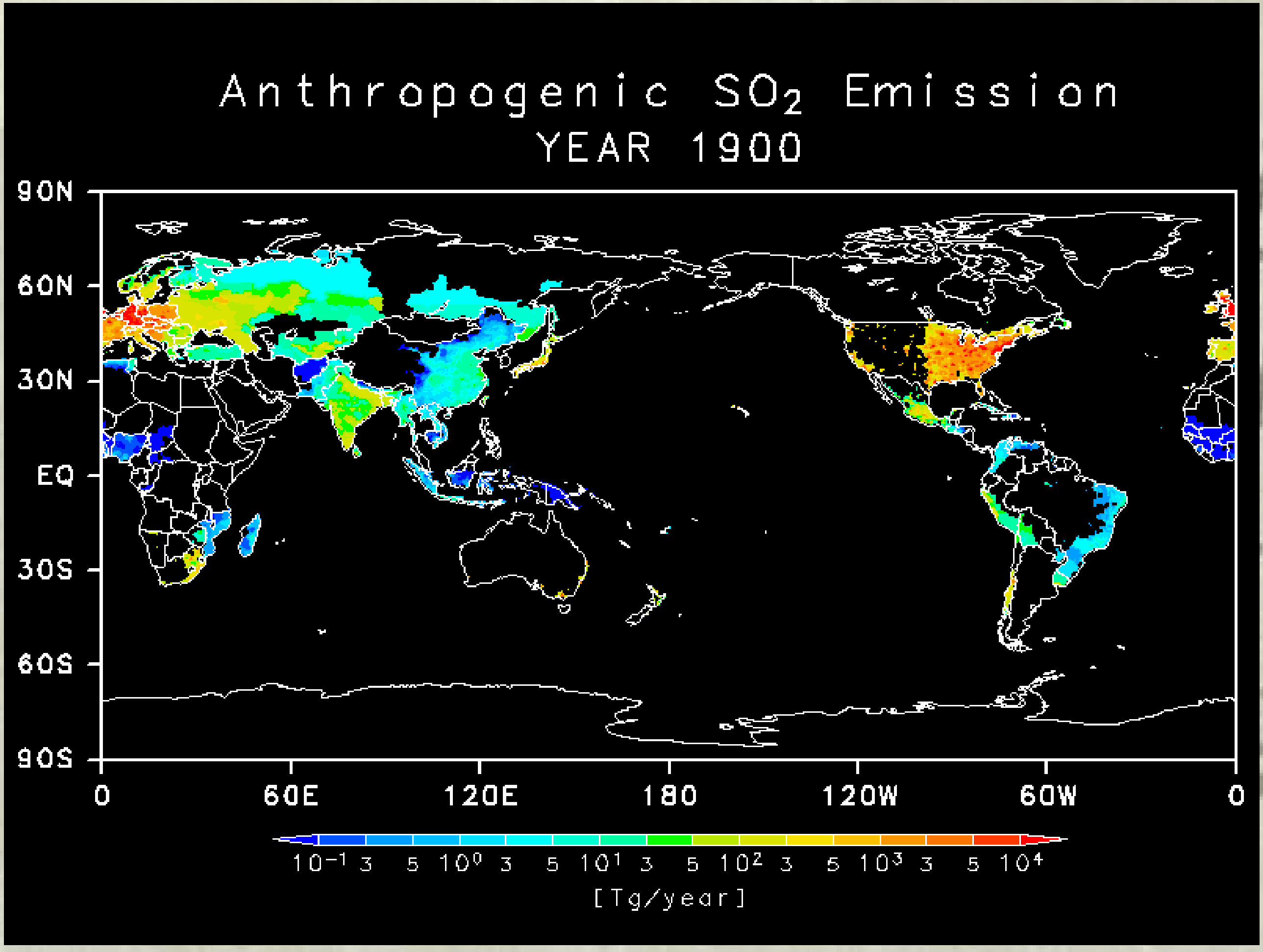

Emission data

Historical Emission of Anthropogenic Black Carbon

- Cou
  - ✓ ... ces,
  - ✓ ... ok,
  - ✓
  - ✓
- Grid

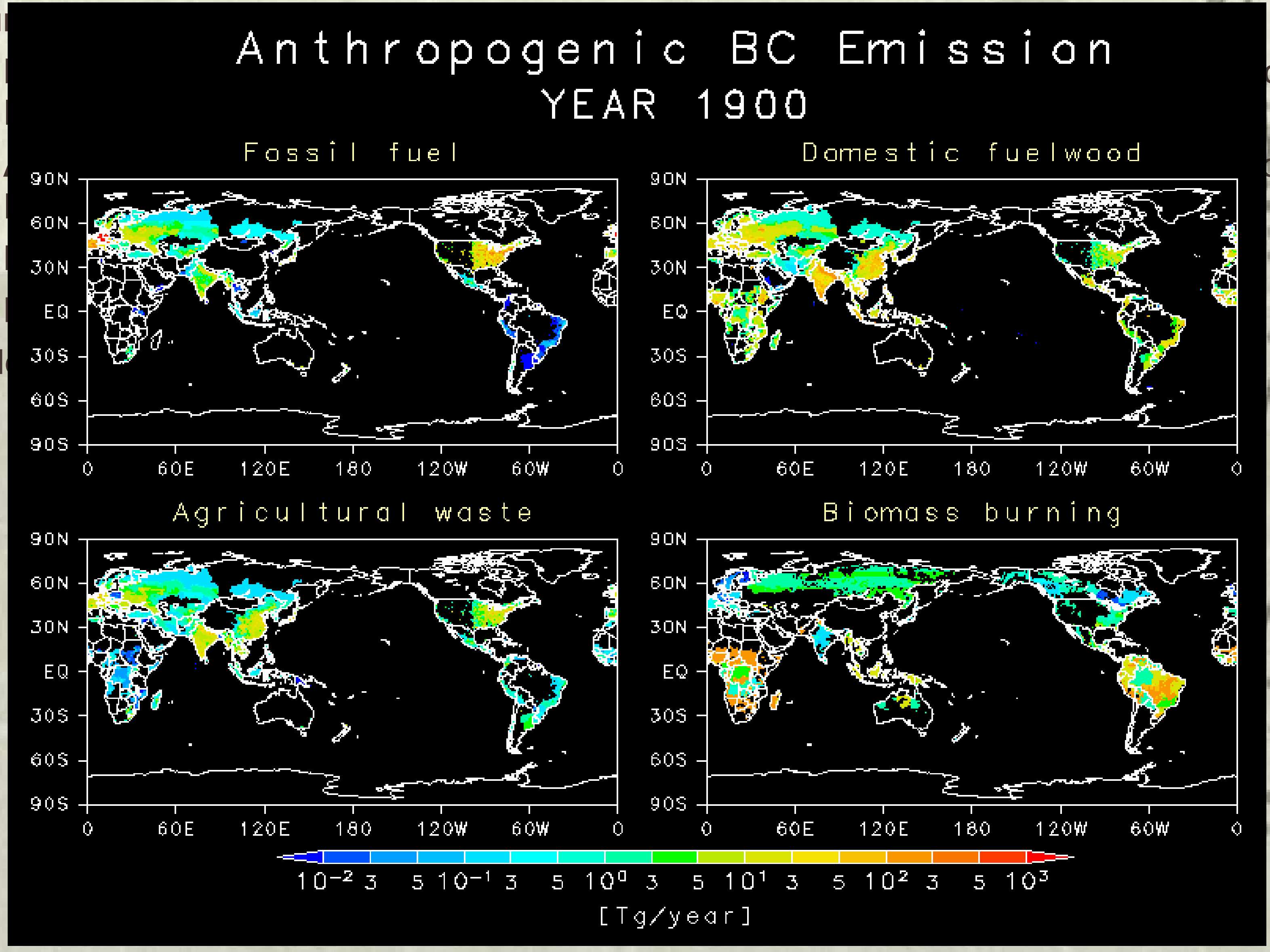

Global aerosol distributions

Optical thickness (550nm)

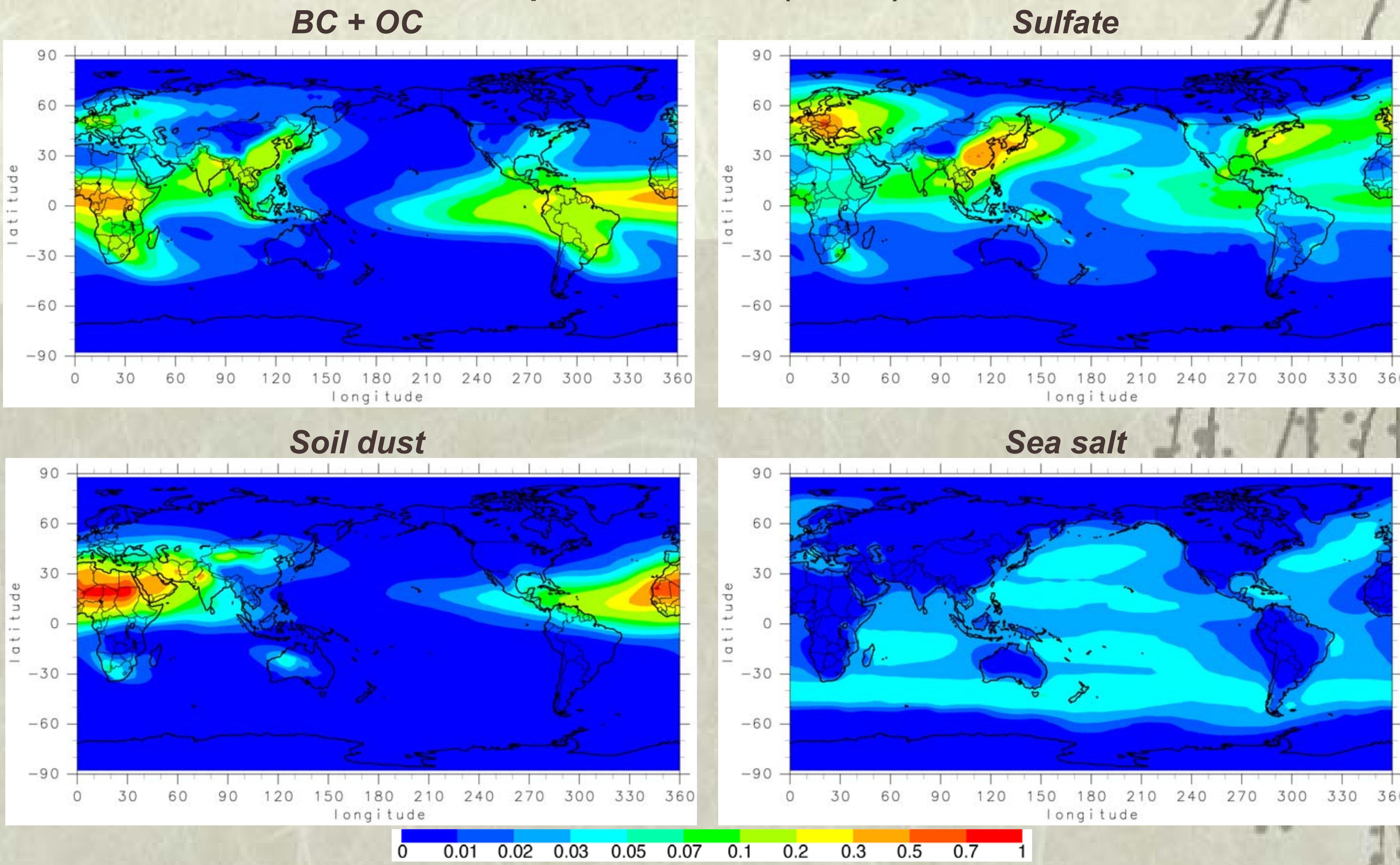

Annual mean distributions of the optical thickness at 550 nm for each aerosol component.

Asian dust storm

April 8 April 12 April 14

TOMS aerosol index *(NASA GSFC)*

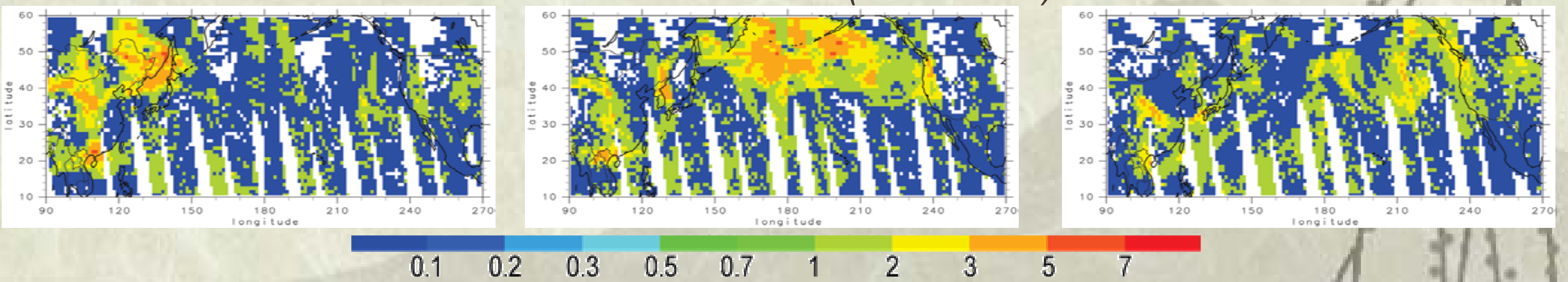

SPRINTARS optical thickness (dust)

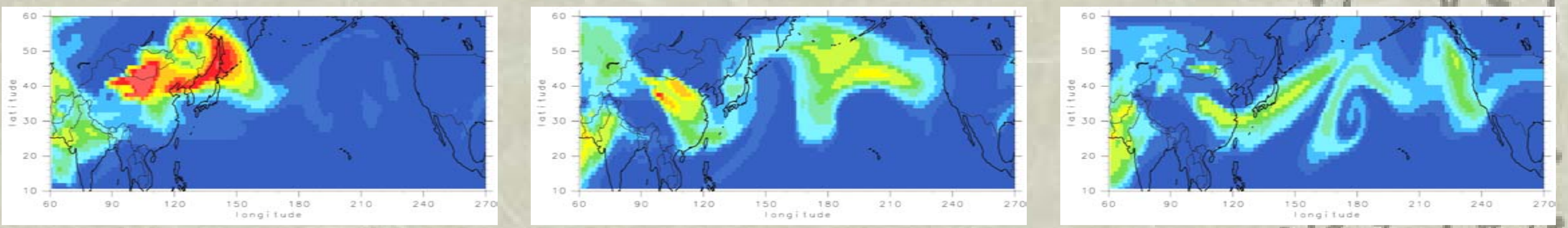

SPRINTARS optical thickness (carbon+sulfate)

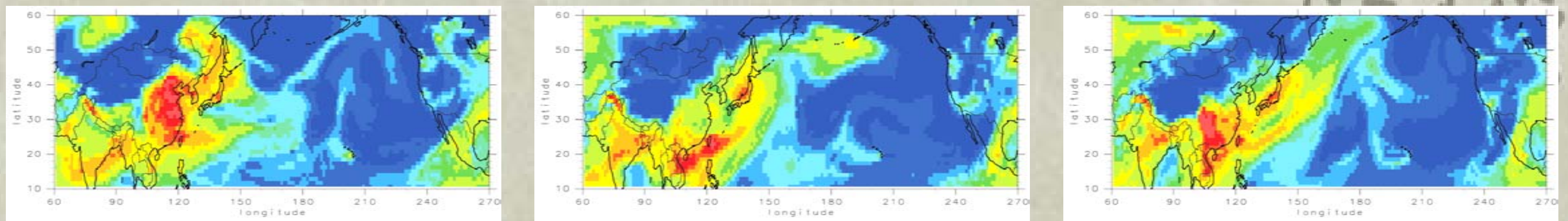

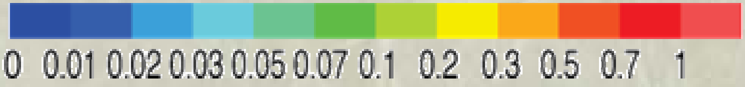

TOMS aerosol index (top) and SPRINTARS optical thickness of soil dust (middle) and carbonaceous plus sulfate aerosols (bottom) from April 8 to 14, 2001 over North Pacific region (*Takemura et al., Geophys. Res. Lett., 2002GL016251, 2002*).

Comparison with observation in Asia

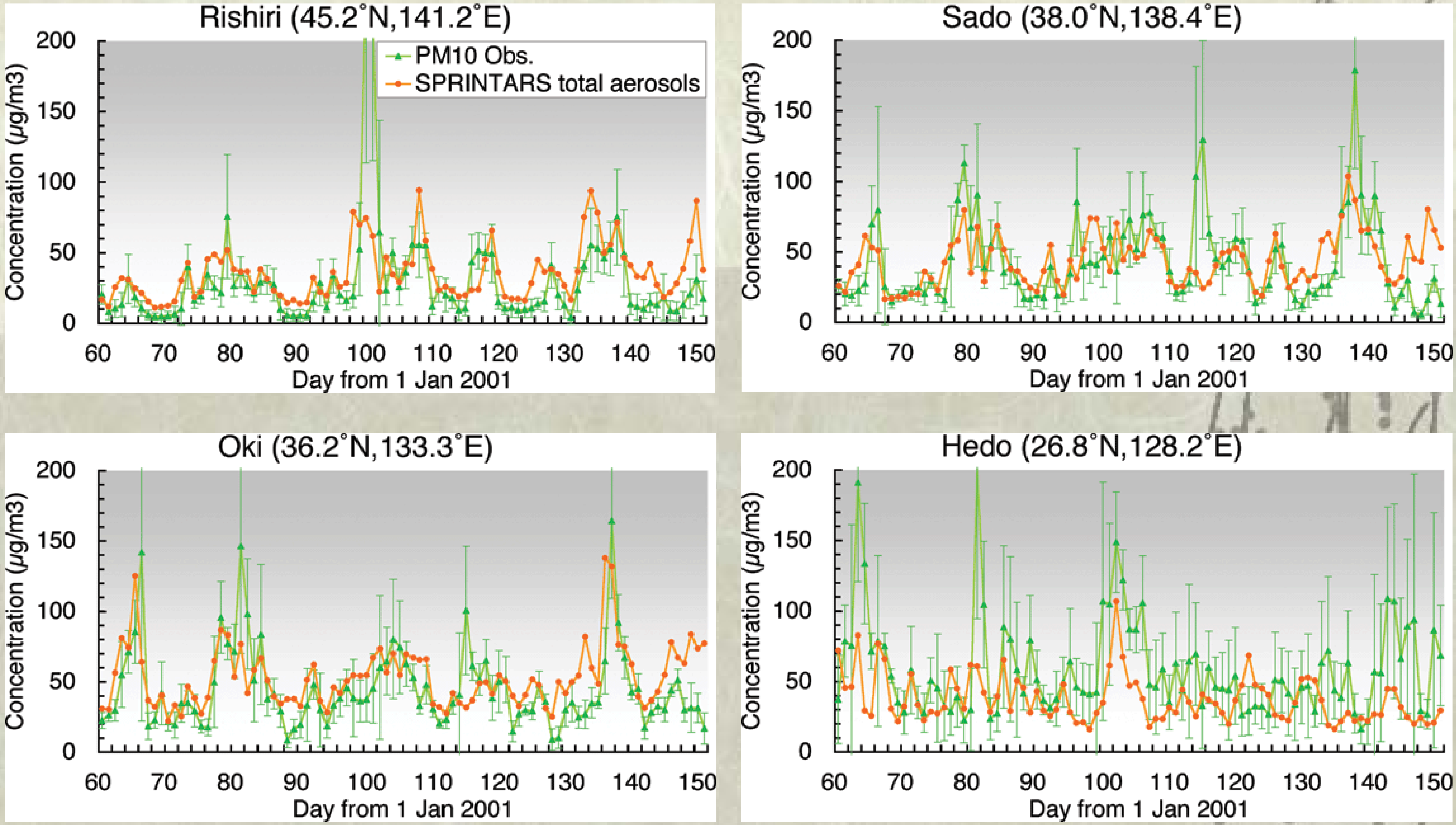

Comparisons with the total aerosol mass concentration simulated by SPRINTARS with observations of the PM10 concentration from 1 March to 31 May 2001 in Japan.

Aerosol particle and cloud droplet number concentrations

Aerosol particle number concentration

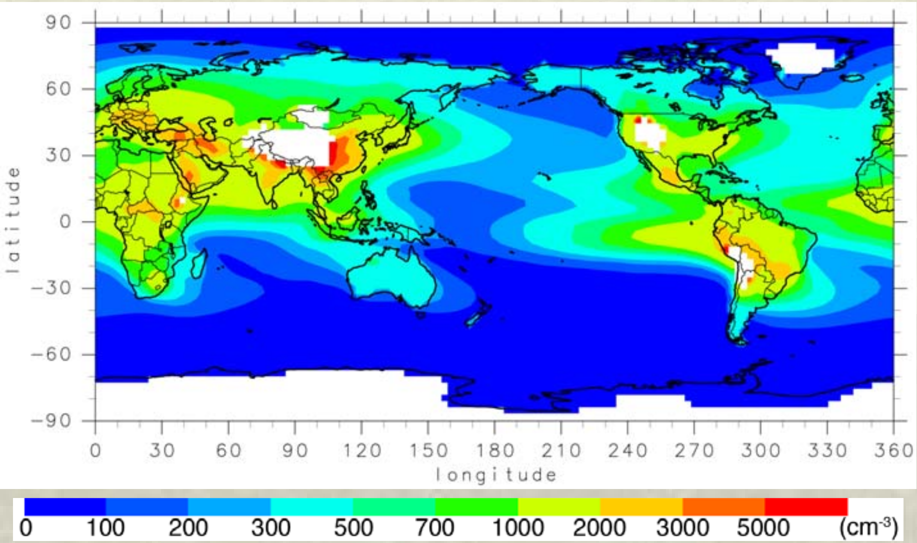

Cloud droplet number concentration

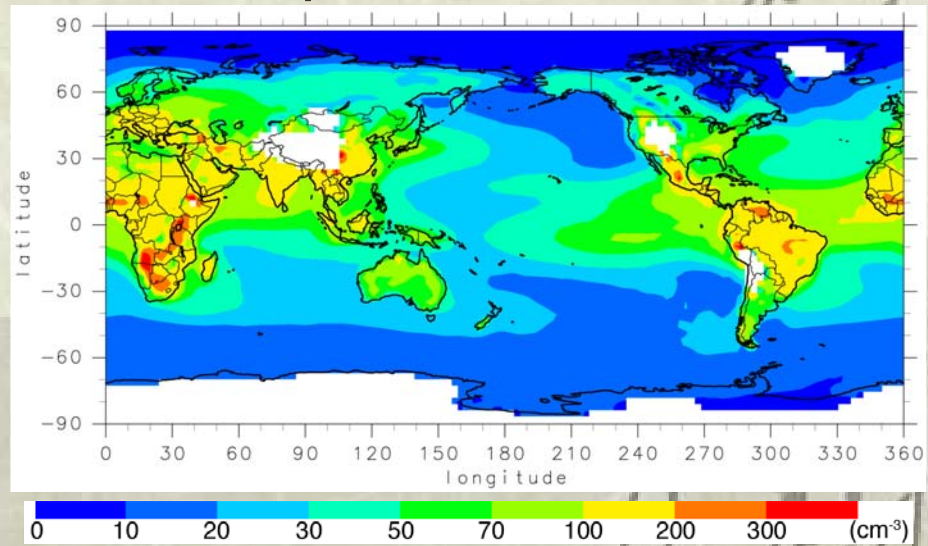

Annual mean distributions of the number concentrations of aerosol particles (left) and cloud droplets (right) at 850 hPa.

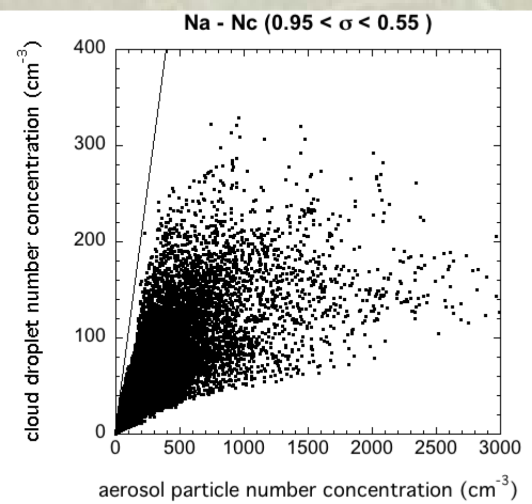

Relationship between the number concentrations of aerosol particles and cloud droplets.

(cf.) past study

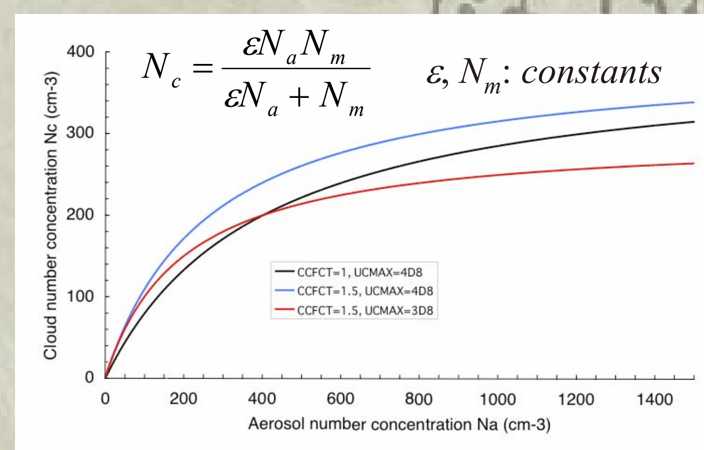

Cloud droplet effective radius

Cloud droplet effective radius (water)

SPRINTARS

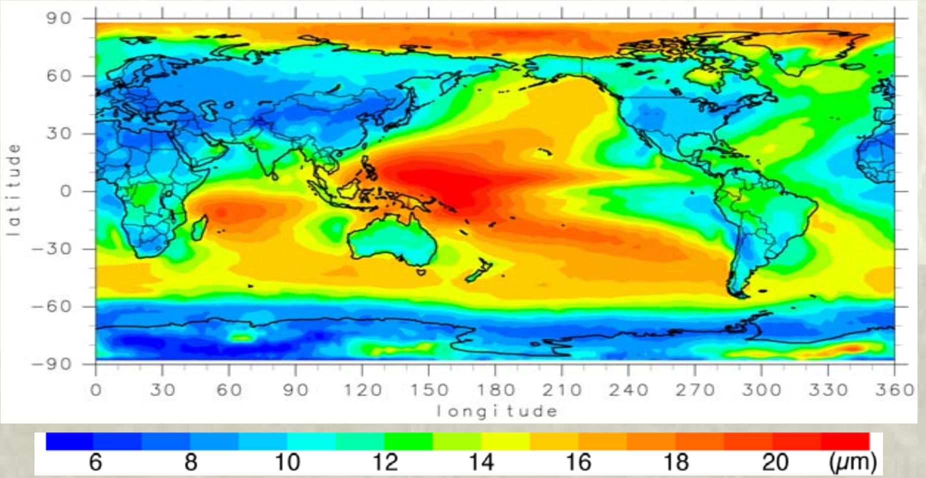

AVHRR (*T. Y. Nakajima*)

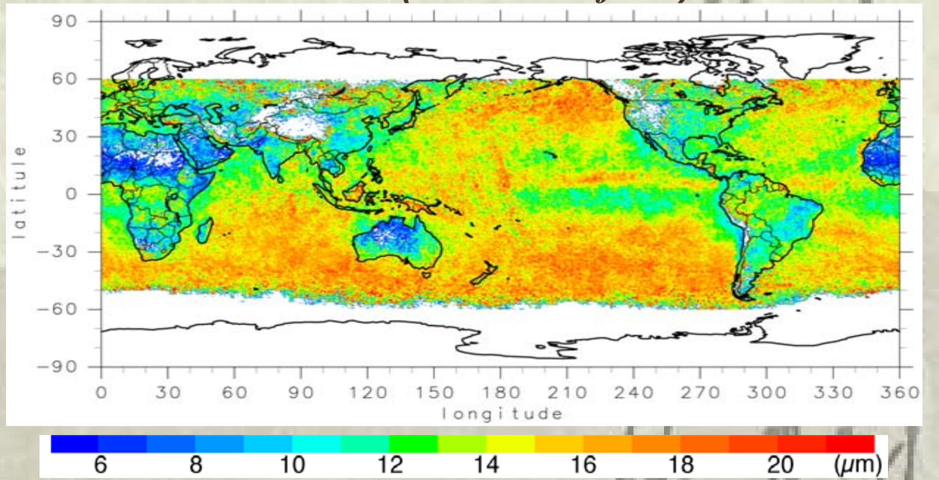

Annual mean distribution of the cloud droplet effective radius at cloud top (T>273K) by SPRINTARS (left) and AVHRR retrieval (right).

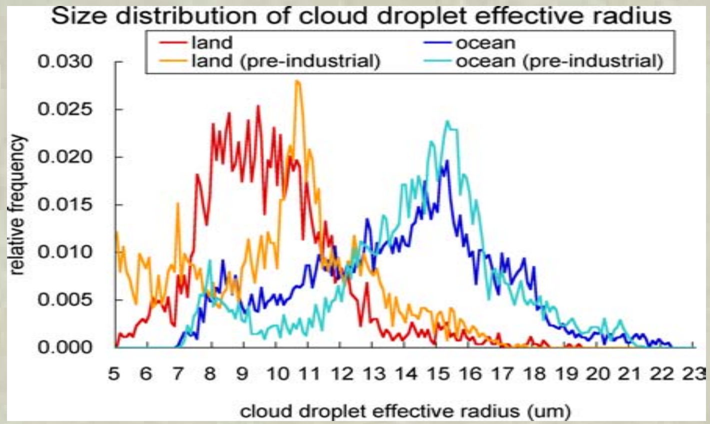

Size distributions of the cloud droplet effective radius at cloud top (T>273K).

Comparison of the cloud droplet effective radius at cloud top (T>273K) between SPRINTARS and AVHRR retrieval.

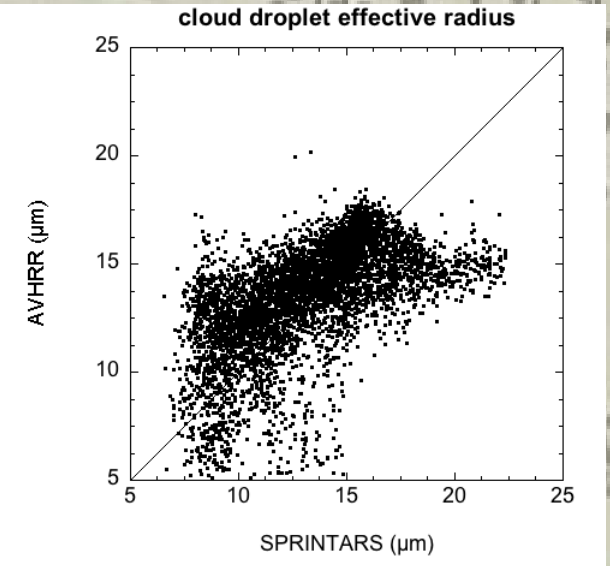

Cloud water and precipitation

Liquid water path

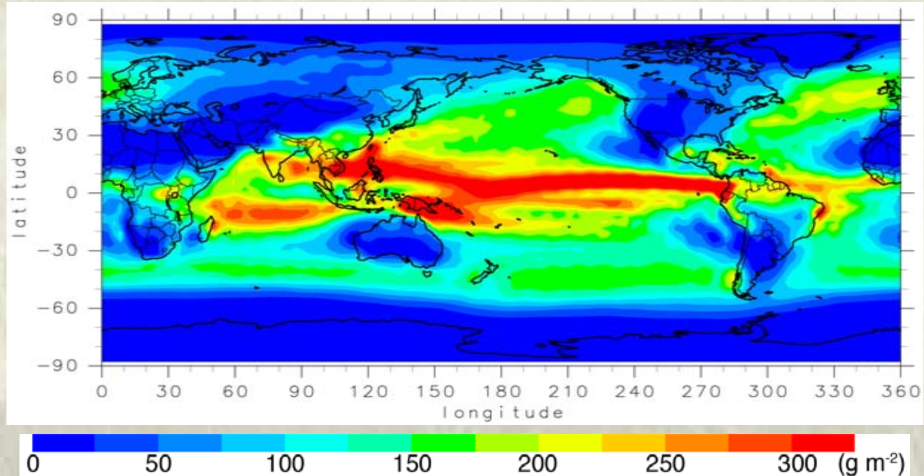

Annual mean distribution of the cloud water path.

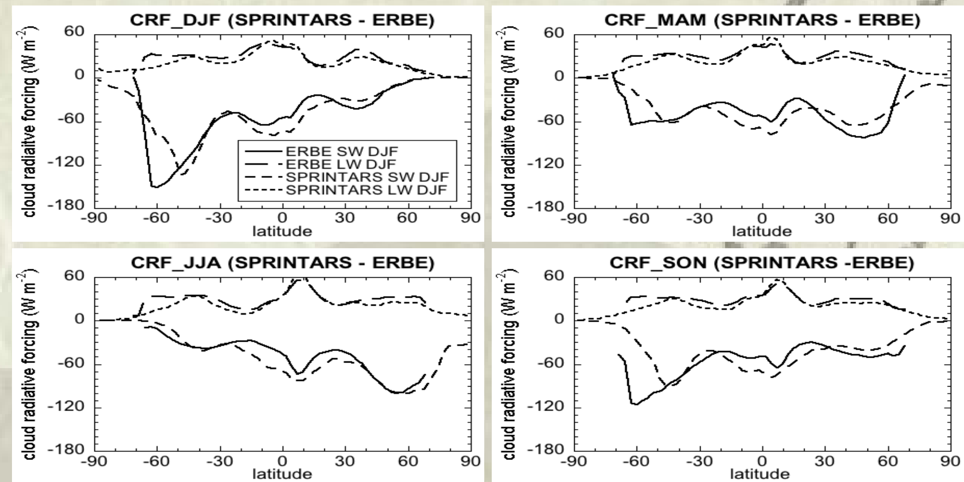

Comparisons of the zonal seasonal mean cloud radiative forcing between SPRINTARS and ERBE.

Precipitation

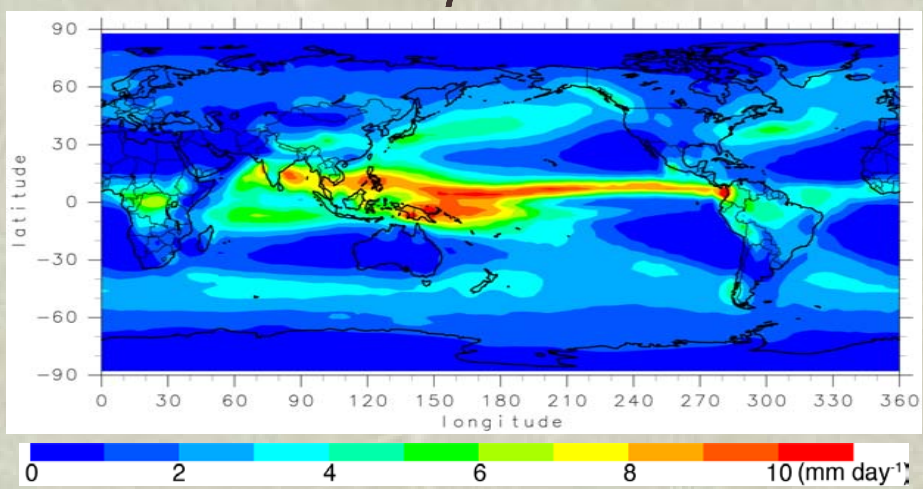

Annual mean distribution of the precipitation.

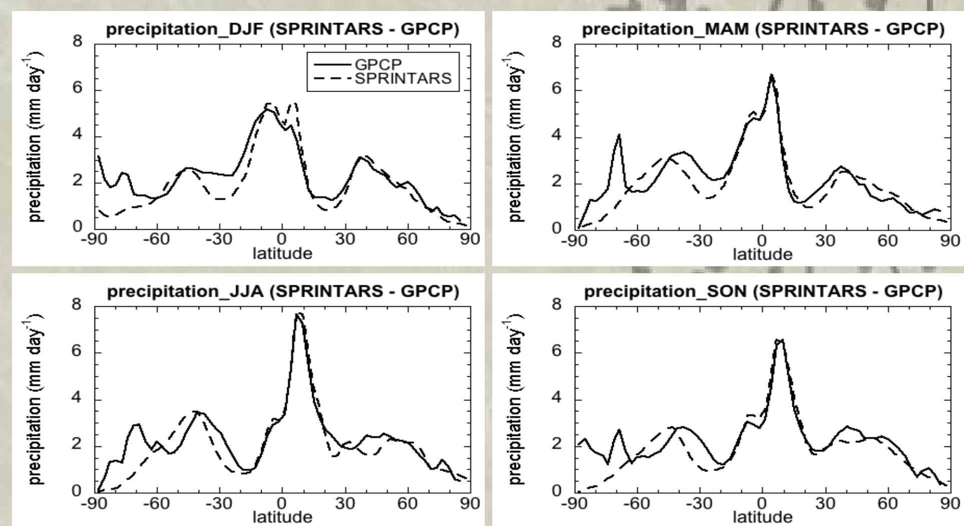

Comparisons of the zonal seasonal mean precipitation between SPRINTARS and GPCP.

Change in cloud parameters

Change in cloud droplet effective radius

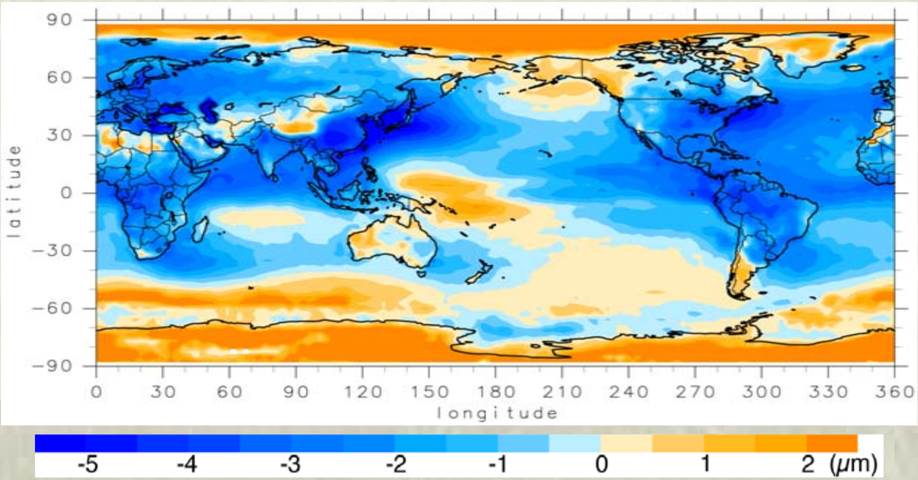

Change in liquid water path

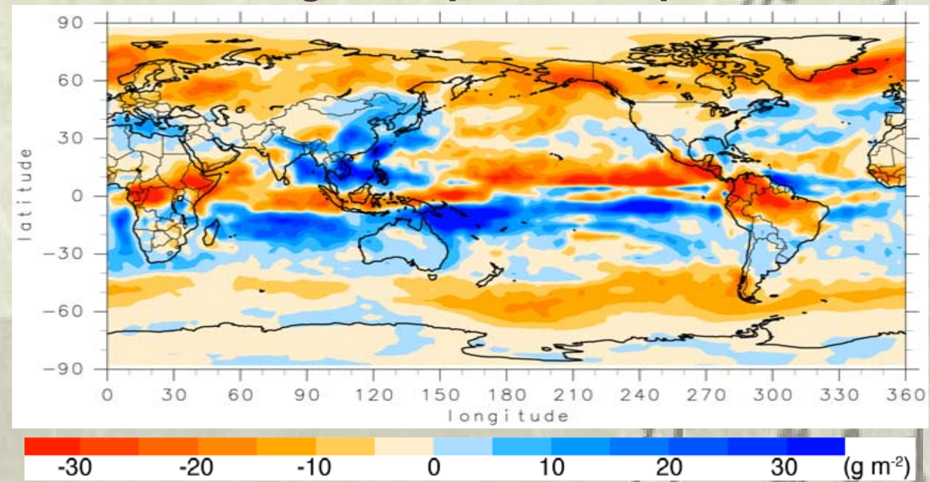

Change in the cloud droplet effective radius (top left), cloud water path (top right), and precipitation (bottom) from pre-industrial to present day.

Change in precipitation

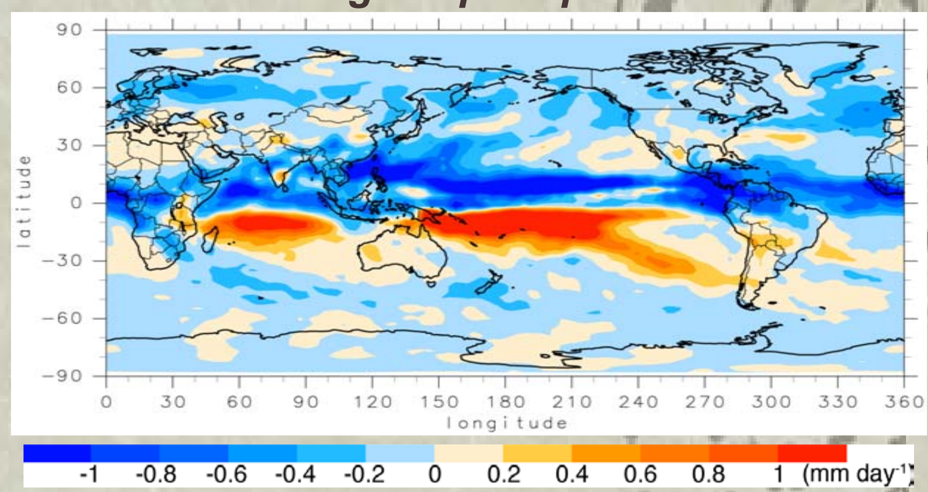

- Decrease in the cloud droplet effective radius due to anthropogenic aerosols (1st indirect effect) is seen almost all over the world, especially in industrial and biomass burning regions.
- Changes in the cloud water and precipitation indicate a change in the hydrological cycle due to the cooling effect by aerosol direct and indirect effects rather than the 2nd indirect effect itself especially over tropical regions.
- The strong signal of the 2nd indirect effect is shown over the east and southeast Asia, and north and tropical Atlantic, which is an increase in the cloud water and a decrease in the precipitation.

Aerosol radiative forcing

Direct radiative forcing ***AVG. –0.14 W m^{-2}***

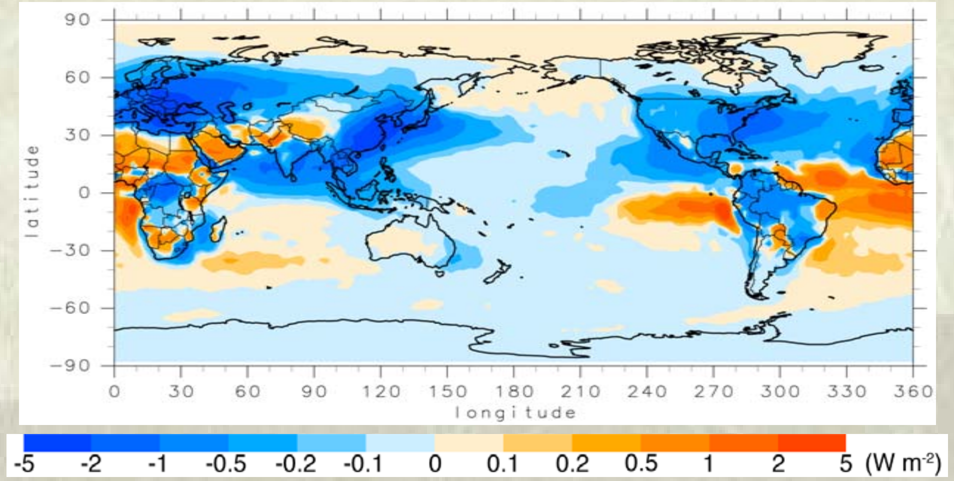

Indirect radiative forcing ***AVG. –0.78 W m^{-2}***

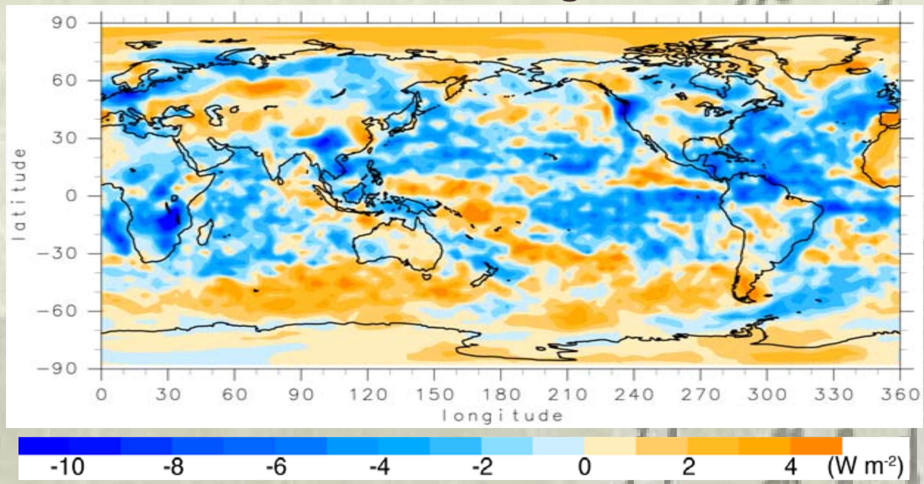

Annual mean distributions of the direct (left) and indirect (right) radiative forcings from pre-industrial and present day. (These results are from the fixed SST and sea ice run.)

Temperature change by aerosol effects

Change in the surface air temperature due to the aerosol effects from pre-industrial and present day.

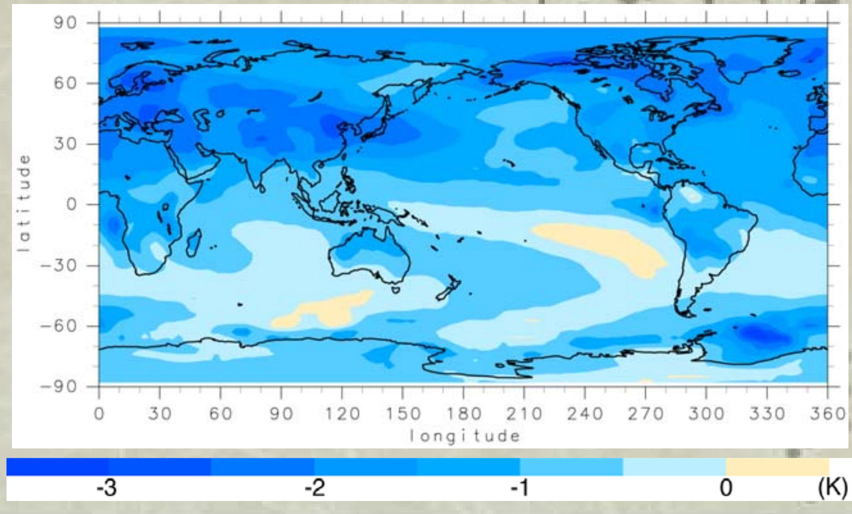

Change in the global mean surface air temperature from 1850 to 2000 by SPRINTARS due to

Aerosols: –1.0 K.

Greenhouse gases: +2.3 K.

→Aerosols cancel one-third to half of the global warming by greenhouse gases.

Climate simulation in the 20th century by CGCM

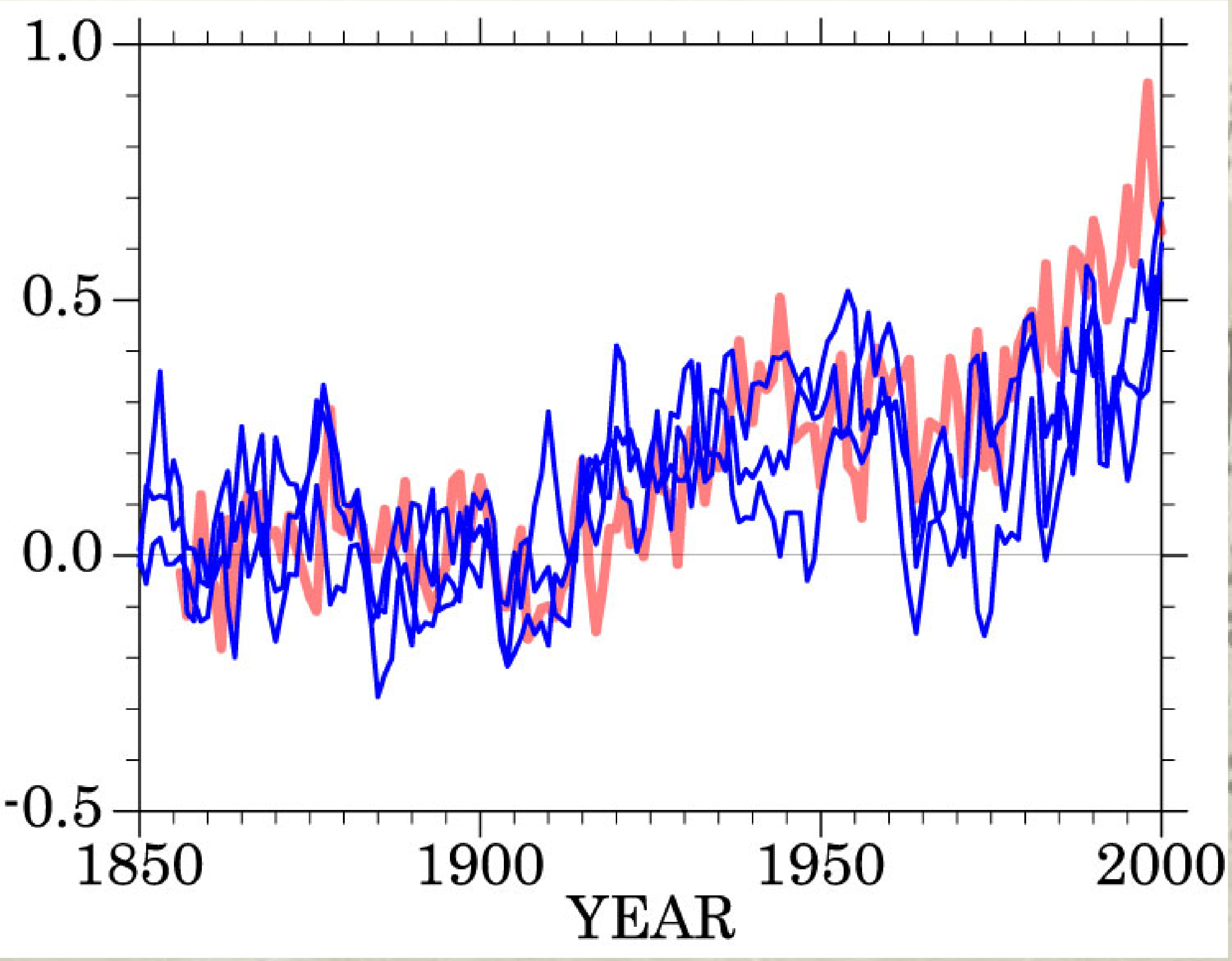

Change in surface air temperature from 1850 to 2000 by the observation (red) and the simulation of ocean-atmosphere general circulation model with the on-line SPRINTARS (blue).

Aerosol budget

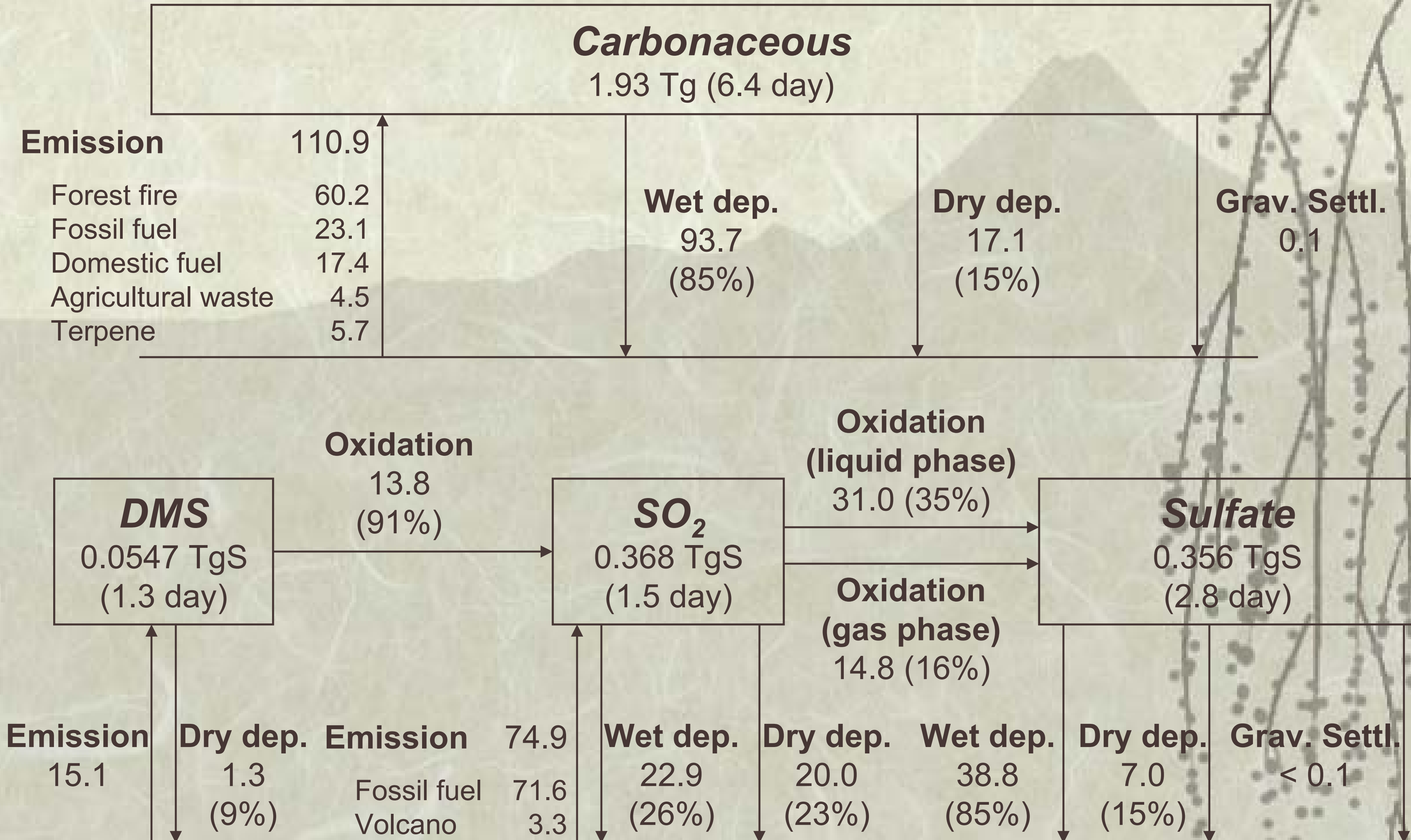

Global total budgets (Tg(S) yr^{-1}) and column loadings (Tg(S)). Parentheses under each budget indicate the ratio of the total fluxes. Those under each column loading indicate the lifetimes.

Aerosol budget

Soil Dust

24.1 Tg (1.7 day)

Emission
5182

Wet dep.
692
(13%)

Dry dep.
3772
(73%)

Grav. Settl.
718
(14%)

Sea Salt

7.87 Tg (0.71 day)

Emission
4036

Wet dep.
2028
(50%)

Dry dep.
1836
(45%)

Grav. Settl.
172
(5%)

Global total budgets (Tg yr^{-1}) and column loadings (Tg). Parentheses under each budget indicate the ratio of the total fluxes. Those under each column loading indicate the lifetimes.

Global aerosol optical properties

Optical thickness (550nm)

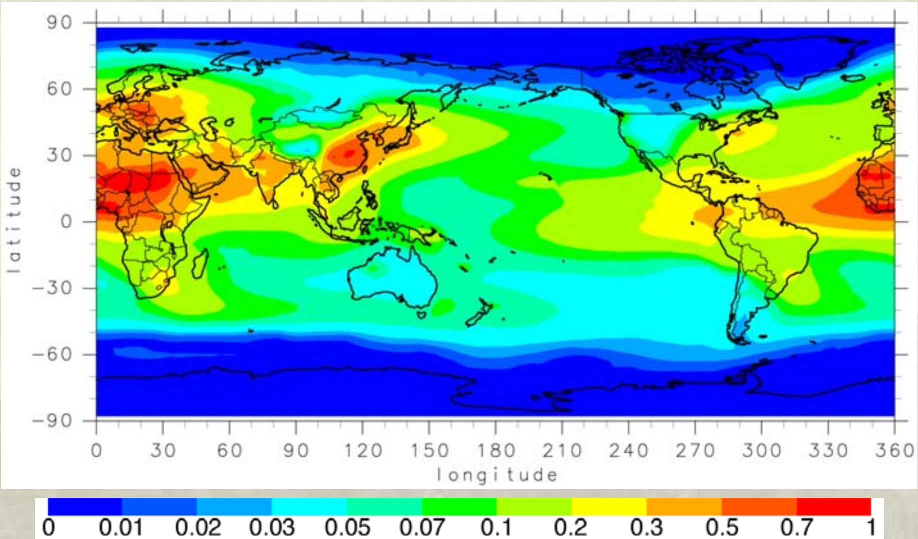

Ångström exponent

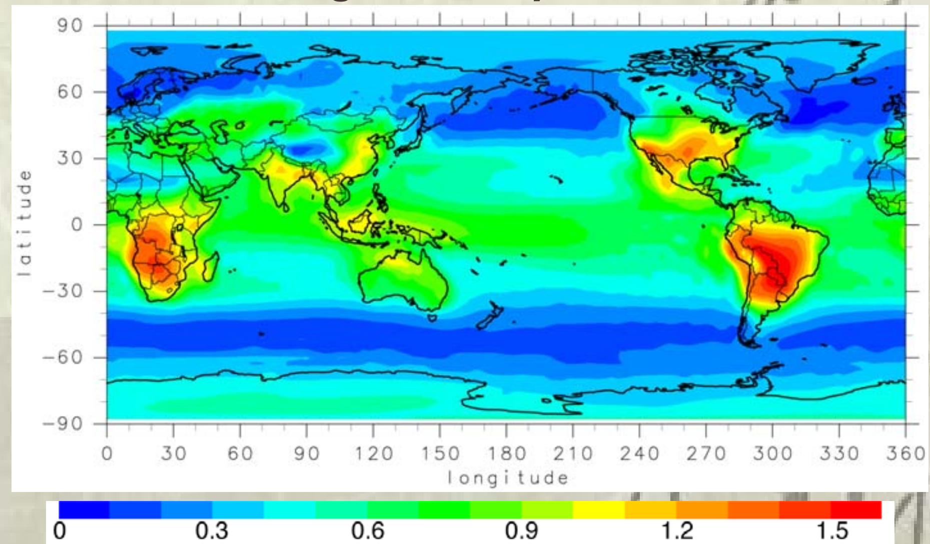

Annual mean distributions of the aerosol optical thickness at 550 nm (top left), Ångström exponent (top right), and single scattering albedo at 550 nm (bottom).

Single scattering albedo (550nm)

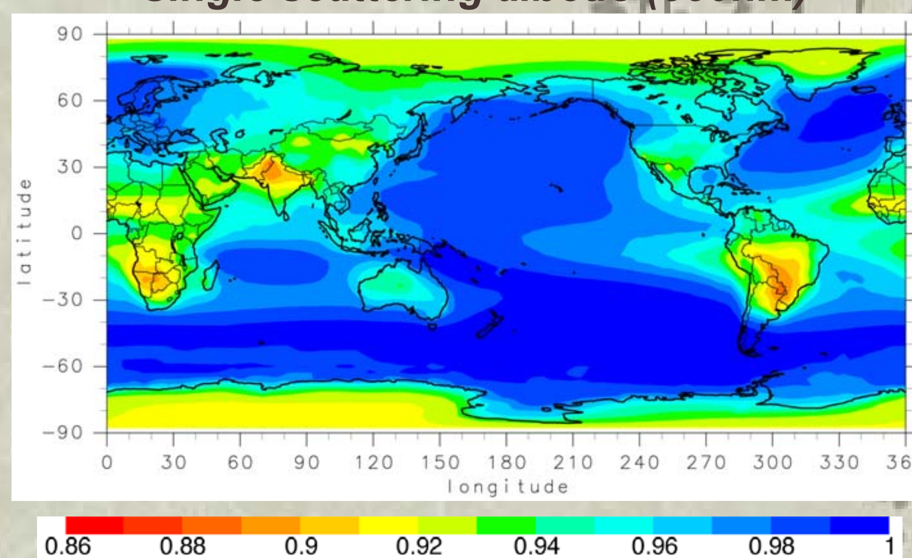

The aerosol optical properties are simulated well by SPRINTARS in comparison with satellite (e.g., AVHRR, SeaWiFS, TOMS), ground-based (e.g., AERONET, SKYNET), and aircraft (e.g., C-130 in ACE-Asia) observations (*Takemura et al. 2002a, 2002b, 2003*).

Comparison with AERONET

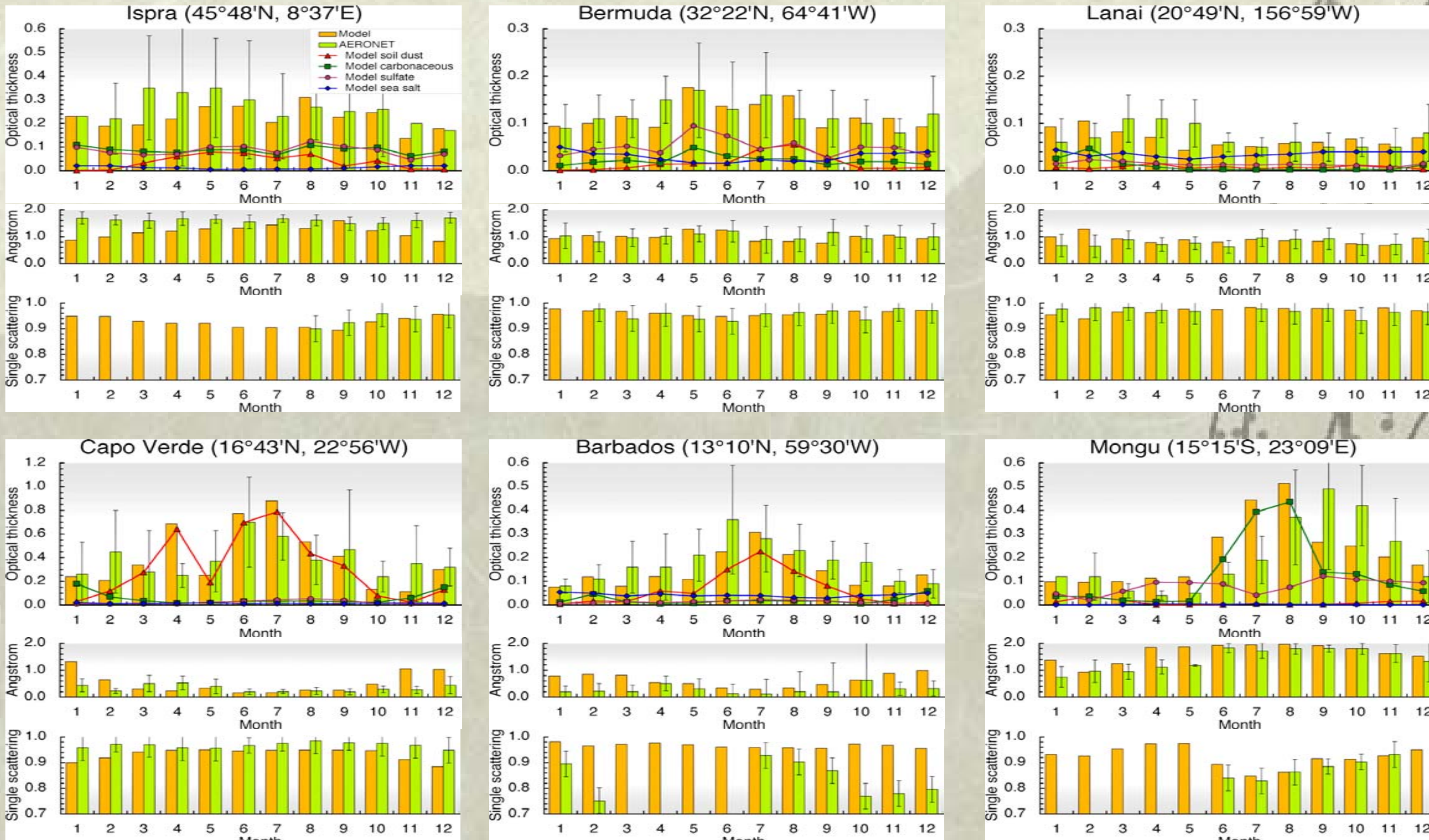

Comparisons of the monthly mean aerosol optical thickness at 550 nm, Ångström exponent, and single scattering albedo at 550 nm simulated by SPRINTARS with AERONET (*Takemura et al. 2002*).